Vacuum xxx (2013) 1–5

Contents lists available at ScienceDirect

Vacuum

journal homepage: www.elsevier.com/locate/vacuum

# Catalytic nature of under- and hetero-coordinated atoms resolved using zone-selective photoelectron spectroscopy (ZPS)

Yanguang Nie [a,b], Yan Wang [a,c,**], Xi Zhang [b,d], Jisheng Pan [e], Weitao Zheng [f], Chang Q. Sun [b,*]

[a] School of Information and Electronic Engineering, Hunan University of Science and Technology, Xiangtan 411201, China
[b] NOVITAS, Nanoelectronics Centre of Excellence, School of Electrical and Electronic Engineering, Nanyang Technological University, Singapore 639798, Singapore
[c] Key Laboratory of Low-dimensional Materials and Application Technology and Faculty of Materials, Optoelectronics and Physics, Xiangtan University, Xiangtan 411105, China
[d] Center for Coordination Bond and Electronic Engineering, College of Materials Science and Engineering, China Jiliang University, Hangzhou 310018, China
[e] Institute of Materials Research and Engineering, ASTAR, Singapore 117602, Singapore
[f] School of Materials Science, Jilin University, Changchun 130012, China

ARTICLE INFO

*Article history:*
Received 18 May 2013
Received in revised form
15 July 2013
Accepted 16 July 2013

*Keyword:*
Surface
Interface
Defect
Catalysis
Binding energy
Bond relaxation

ABSTRACT

We present an approach for distillation of the coordination-resolved electronic binding energy and bond relaxation dynamics, which has enabled clarification of the catalytic nature of under- and hetero-coordinated atoms. It is classified that Pt adatoms and CuPd alloy serve as acceptor-type catalysts because of the bond-order-deficiency induced quantum entrapment while Rh adatoms and AgPd alloy serve as donor-type catalysts because of the polarization of the conduction electrons of the adatoms by the densely, locally entrapped core electrons. This technique also enables the distillation of the polarized electronic states of graphite point defects and the entrapped states of the monolayer skin of graphite, which may serve, respectively, donor- and acceptor-type catalyst. The developed approach complements scanning tunneling microscopy/spectroscopy and photoelectron spectroscopy for the atomistic, local, and quantitative information of bond and electronic relaxation dynamics.



Under-coordinated adatoms or atoms at sites surrounding defects, terrace edges, surfaces, and hetero-coordinated atoms associated with impurities and interfaces demonstrate fascinating properties that could not be observed in bulk materials. The behavior of electrons of such ill-coordinated atoms has enabled new catalysts [1,2] with desiring of physical mechanisms. Resolving the behavior of bonds and electrons associated with such ill-coordinated atoms at the atomic scale is beyond available techniques such as scanning tunneling microscope/spectroscopy (STM/S) and photoemission spectroscopy (PES). STM/S maps local electrons in the open side of a *too-thin* subatomic layer of a surface with energies of a few eVs cross Fermi energy ($E_F$) [3–5]. PES probes statistic and volumetric information of electrons with binding energy in the valence band and below within a *too-thick* layer of 10 nm or thicker [6–9]. Therefore, the local and quantitative information regarding the bond length and energy and electronic relaxation dynamics from atomistic sites is a great challenge.

In this communication, we present a zone-selective photoelectron spectroscopy (ZPS) [10] for the coordination-resolved electronic binding energy, which enables the classification of the catalytic nature of the ill-coordinated systems such as Rh and Pt adatoms, AgPd and CuPd interface alloys and the point defects and the monolayer skin of graphite. We emphasize that the ill-coordination induced bond relaxation and the associated quantum entrapment and polarization dictates the performance of electrons of these ill-coordinated atoms.

One can imagine the outcome of differentiating two spectra of a certain energy band collected: (i) from the same defect-free surface at different emission angles (the angle between surface normal and the photoelectrons); (ii) from the same surface after and before the surface is being conditioned such as creating defects or adding

* Corresponding author.
** Corresponding author. School of Information and Electronic Engineering, Hunan University of Science and Technology, Xiangtan 411201, China.
*E-mail addresses:* ywang8@hnust.edu.cn (Y. Wang), Ecqsun@ntu.edu.sg (C.Q. Sun).

0042-207X/$ – see front matter © 2013 Elsevier Ltd. All rights reserved.
http://dx.doi.org/10.1016/j.vacuum.2013.07.025

guest atoms under the same measurement conditions; or (iii) from different specimens containing the same constituent element. Upon the standard processes of background correction and spectral peak area normalization, the ZPS in (i) keeps the spectral features due to the skin by filtering out the bulk information as the XPS collects more information from the surface at larger emission angles [11]. Likewise, the ZPS in (ii) purifies merely the spectral features due to conditioning. The ZPS in (iii) resolves the alloying effect on the energy shifts of the respective levels. The ZPS also filters out all the artifact background such as the charging effect and the "initial–final states" relaxation effect that exist throughout the course of measurements. This technique can be used for monitoring surface and interface processes such as crystal growth, defect generation, chemical reaction, alloy formation, etc., both statically and dynamically.

Procedures employed in the ZPS include: (i) collects the referential XPS spectrum from a clean surface at an angle approaching the surface normal and a plural of spectra from the surface at larger emission angles or from the same surface being conditioned or alloyed; (ii) subtracts the referential spectra from the ones to be examined upon proper background correction and peak area normalization under the guideline of spectral area conservation. The rule of peak area conservation guarantees that the integration of each spectrum is proportional across to eliminate the scattering effect.

The ZPS is developed based on the bond order–length–strength (BOLS) correlation [12] and the nonbonding electron polarization (NEP) [13] mechanisms: Firstly, the core-level energy shift from that of an isolated atom is dominated by the crystal potential in the Hamiltonian and the extent of the shift is proportional to the cohesive energy per bond at equilibrium. Secondly, bonds between under-coordinated atoms become shorter and stronger, which results densification and entrapment of the core electrons and their binding energies. Thirdly, the nonbonding electrons such as the dangling bond electrons in carbon or the otherwise conduction electrons of the noble metals will be polarized by the densely entrapped core electrons. Finally, the polarized electron will in turn split and screen the crystal potential to the core level electrons. The BOLS correlation is global but the NEP is subject to the presence of the nonbonding electrons. Hetero-coordinated atoms may follow the BOLS-NEP or the opposite – bond becomes longer and softer, which cause negative shift of the energy levels.

Therefore, a combination of the BOLS-NEP and the band theory [14] formulates the energy shift of the $\nu$th core level in the following Hamiltonian:

$$H = \left[-\frac{\hbar^2\nabla^2}{2m} + V_{\mathrm{atom}}(r)\right] + V_{\mathrm{cry}}(r)(1+\Delta_{\mathrm{H}})$$

The intra-atomic potential $V_{\mathrm{atom}}(r)$ determines the $\nu$th core level energy of an isolated atom, $E_\nu(0)$, and the crystal potential $V_{\mathrm{cry}}(r)$ determines the core level shift $\Delta E_\nu(x)$. They follow the relations [14,15],

$$\begin{aligned} E_\nu(0) &= \langle \nu,i|V_{\mathrm{atom}}(r)|\nu,i\rangle \\ \Delta E_\nu(x) &= \langle \nu,i|V_{\mathrm{cry}}(r)(1+\Delta_{\mathrm{H}})|\nu,i\rangle\left[1+\frac{z\langle \nu,i|V_{\mathrm{crym}}(r)(1+\Delta_{\mathrm{H}})|\nu,j\rangle}{\langle \nu,i|V_{\mathrm{cry}}(r)(1+\Delta_{\mathrm{H}})|\nu,i\rangle}\right] \\ &\cong E_{\mathrm{b}}(1+\Delta_{\mathrm{H}})\left(1+\left(\frac{\text{overlap integral}}{\text{exchange integral}}<3\%\right)\right) = E_x \end{aligned} \quad (1)$$

where $|\nu,i\rangle$ is the eigen wave function at the ith atomic site. $\langle \nu,i|\nu,j\rangle = \delta_{ij}$ because of the strong localization of the core electrons. $E_{\mathrm{b}}$ and $E_x$, respectively, represent the single bond energy in

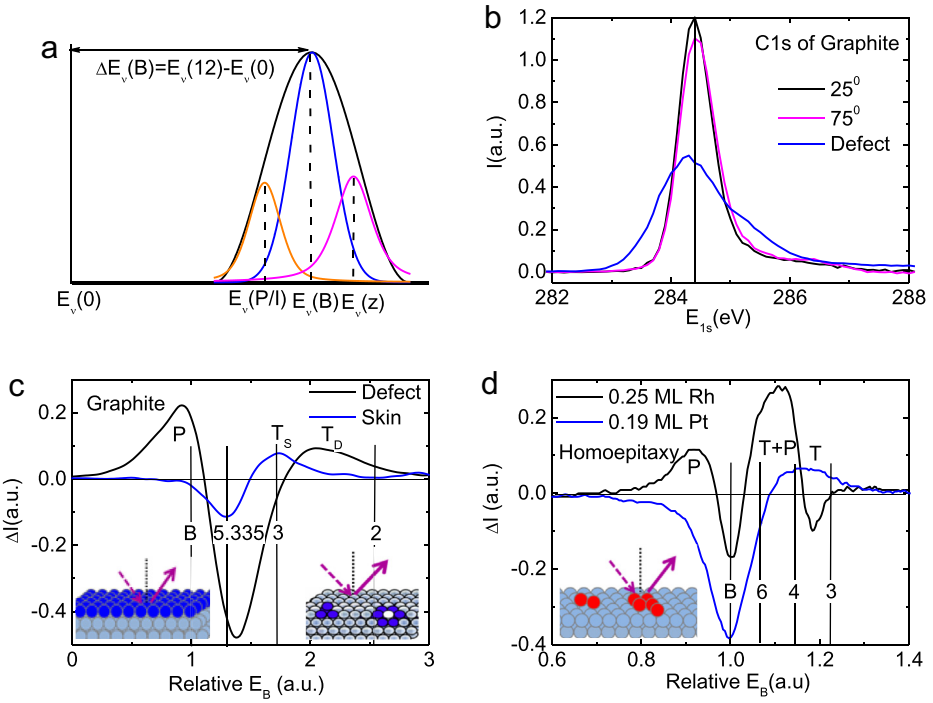


**Fig. 1.** (a) Decomposition of XPS spectrum with components of the bulk, polarization and the $z$-coordinated atoms. (b) Normalized XPS of graphite defect-free surface at emission angles of 25° and 75°, and defected surface with vacancy concentration of $8.4 \times 10^{-16}$ cm$^{-2}$. (c) ZPS profiles for the monolayer skin and point defect of graphite surface with global entrapment and defect polarization. (d) ZPS profiles for Pt and Rh adatoms showing the entrapment dominance of Pt and polarization presents for Rh, being similar to graphite skin and defect, respectively. The $x$-axes in (c) and (d) are set as dimensionless unity of $[E - E_{\mathrm{c}}(0)]/[\Delta E(\mathrm{B})]$ for convenient view. Results confirm that undercoordination shortens and strengthens the bonds between undercoordinated atoms associated with subjective polarization of the nonbonding states.

Please cite this article in press as: Nie Y, et al., Catalytic nature of under- and hetero-coordinated atoms resolved using zone-selective photoelectron spectroscopy (ZPS), Vacuum (2013), http://dx.doi.org/10.1016/j.vacuum.2013.07.025

**Table 1**
BOLS-ZPS derived effective atomic CN($z$), bond length $d_z$, bond energy $E_z$, and the binding energy of the under-coordinated atoms. $C_z$ is the bond contraction coefficient.

| | $z$ | $C_z$ | $d_z$ (nm) | $E_z$ (eV) | $E_\nu$ (eV) | $P$ (eV) |
|---|---|---|---|---|---|---|
| C atom | 0 | – | – | – | 282.57 | |
| Graphite vacancy | 2.20 | 0.73 | 0.112 | 1.383 | 285.54 | 283.85 |
| | 2.40 | 0.76 | 0.116 | 1.262 | 285.28 | |
| Graphite monolayer skin | 3.10 | 0.82 | 0.127 | 1.014 | 284.75 | |
| Graphite | 5.335 | 0.92 | 0.142 | 0.757 | 284.20 | |
| Pt atom | 0 | – | – | – | 67.50 | |
| Pt adatom | 3.15 | 0.826 | 0.229 | 0.589 | 71.18 | |
| Pt bulk | 12 | 1 | 0.277 | 0.487 | 70.49 | |
| Rh atom | 0 | – | – | – | 302.58 | |
| Rh adatom | 3.0 | 0.817 | 0.220 | 0.586 | 307.51 | 306.21 |
| Rh bulk | 12 | 1 | 0.269 | 0.479 | 306.53 | |

ideal bulk and that under perturbations with $x$ being the index. This definition yields the following relation to determine the $E_\nu(0)$ from the measurement of the coordination-resolved ($z \neq z'$) energy shift,

$$\frac{E_\nu(z)-E_\nu(0)}{E_\nu(z')-E_\nu(0)}=\frac{C_z^{-m}}{C_{z'}^{-m}},\ \text{or}\ E_\nu(0)=\frac{C_{z'}^{m}E_\nu(z')-C_z^{m}E_\nu(z)}{C_{z'}^{m}-C_z^{m}} \tag{2}$$

The following possible effects perturb the Hamiltonian ΔH [15]:

$$\Delta_H=\begin{cases} C_z^{-m}-1=E_z/E_b-1 & \text{(Entrapment)}\\ (E_\nu(p)-E_\nu(0))/(E_\nu(12)-E_\nu(0))-1 & \text{(Polarization)}\\ (E_\nu(I)-E_\nu(0))/(E_\nu(12)-E_\nu(0))-1 & \text{(Interface)}\end{cases}$$
$$C_z=d_z/d_b=2/\{1+\exp[(12-z)/(8z)]\}\quad\text{(Bond contraction coefficient)} \tag{3}$$

$p$ and $I$ represent the polarization and the interface effect as shown in Fig. 1(a). $C_z$ is the bond contraction coefficient. $E_z$ and $E_b$ is the cohesive energy of bonds associated with $z$-coordinated atoms and in the bulk. $d_b$ and $d_z$ are the respective bond length. The $m$ is the bond nature index that correlates the bond energy and bond length.

Decomposition of the measured XPS data of various surfaces based on the BOLS premise has led to the $z$-dependent core level energy of the following specimens (eV) [15–22]:

$$E_\nu(z)=E_\nu(0)+[E_\nu(12)-E_\nu(0)]C_z^{-m}=\begin{cases}282.57+1.32C_z^{-2.56} & (\text{C 1s})\\ 302.58+3.95C_z^{-1} & (\text{Rh } 3d_{5/2})\\ 67.50+2.99C_z^{-1} & (\text{Pt } 4f_{7/2})\\ 931.00+1.70C_z^{-1} & (\text{Cu } 2p_{3/2})\\ 333.02+4.63C_z^{-1} & (\text{Ag } 3d_{5/2})\\ 330.34+3.98C_z^{-1} & (\text{Pd } 3d_{5/2})\end{cases} \tag{4}$$

For ZPS analysis, we measured the XPS $C_{1s}$ spectra from graphite (0001) surface at different emission angles and with and without point defects created by spraying $Ar^+$ plasma at controllable doses and spraying times [23]. We also measured the UPS and XPS spectra of Cu 2p, Ag 3d, and Pd 3d from the pure metals and their alloys [24].

Fig. 1(b) shows the normalized typical XPS spectra collected from clean graphite (0001) surface at emission angles of 25° and 75° and the same surface with vacancy defect concentration of $8.4\times10^{-16}$ cm$^{-2}$. Fig. 1(c) shows the differential ZPS of the defects and the monolayer skin.

According to principle of ZPS, the area above the $x$-axis represents the gain and the area below is loss of energy states due to the specific point defects or the monolayer skin. The net gain should be zero because of the rule of spectral area (total number of emitted electrons) conservation. The shifting direction of states indicates the electronic or the bond energy gain or loss.

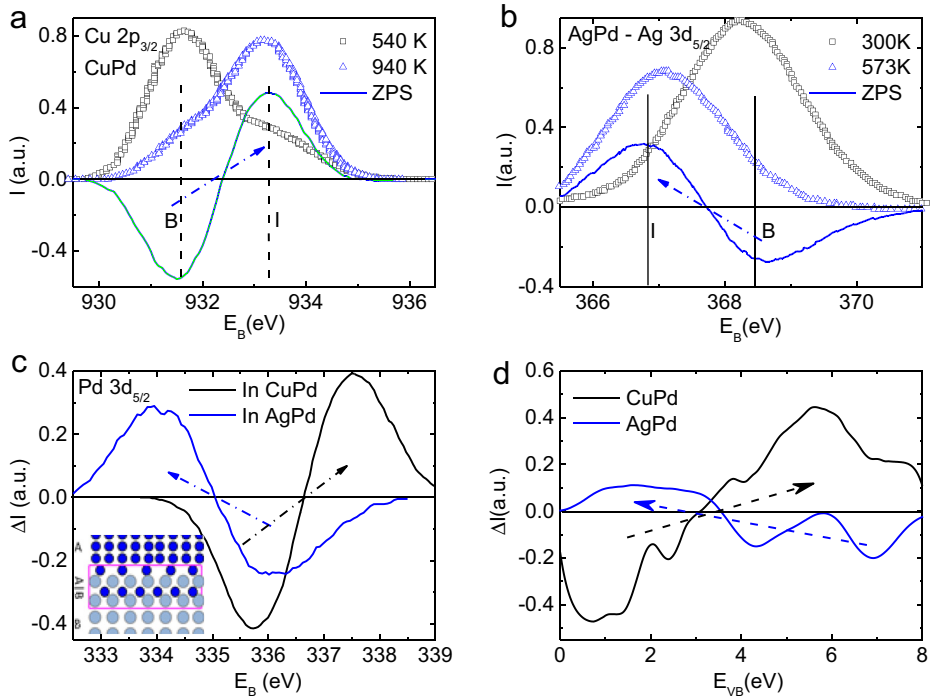


**Fig. 2.** ZPS profiles of (a) Cu $2p_{3/2}$, (b) Ag $3d_{5/2}$, (c) Pd $3d_{5/2}$, (d) the valence bands of the AgPd and CuPd interface alloys. CuPd shows entrapment dominance and the AgPd polarization dominance upon interface formation, and hence clarify their catalytic nature as being acceptor (CuPd) and donor (AgPd) like performance. Thick lines in (a) and (b) are the normalized XPS profiles.

Please cite this article in press as: Nie Y, et al., Catalytic nature of under- and hetero-coordinated atoms resolved using zone-selective photoelectron spectroscopy (ZPS), Vacuum (2013), http://dx.doi.org/10.1016/j.vacuum.2013.07.025

Table 1 summarizes information derived from the BOLS-ZPS analysis. For the monolayer skin, ZPS shows an energy gain, shifting from the bulk valley ($z = 5.335$) [15] to the entrapped states of $T_S$ ($z \sim 3.1$) with bond energy gain of 15%. However, Fig. 1(c) shows that defect creation shifts the entrapped states from $T_s$ of 115% to $T_D$ of 122% with respect to the bulk valley. The effective $z$ for the $T_D$ is ~2.2–2.4, indicating contribution from the next nearest neighbors. Except for the $T_D$ states, a broad peak denoted $P$ emerges with energy 0.31 eV above the bulk valley. With the known energy of $E_{1s}(0)$, 282.57 eV and the bulk shift 1.32 eV in Eq. (4), the polarization coefficient is $p = (283.63 - 282.57)/1.32 = 1.06/1.32 = 0.80$. Surface defect-induced polarization of graphite coincides with that probed using STM [25].

Findings indicate that bonds between surface atoms are shorter and stronger than those inside the bulk and bonds nearby defects are even shorter and stronger than those in the surface. One neighbor loss means a lot because of the polarization effect. According to the BOLS-NEP premise, as the vehicle for the topologic insulator, such Dirac-Fermion at the edges of graphene or at the point defect of graphite results from the polarization of the dangling bond electrons by the locally and densely entrapped core electrons associated with undercoordinated carbon atoms at edges.

Fig. 1(d) compares the ZPS profiles for the Pt and the Rh adatoms derived from the XPS data measured from Rh(110) and Rh(111) surfaces with adatom coverage up to 1/4 ML [26,27]. Results indicate that the entrapment is global but Rh adatoms show the additional polarized states. The ZPS of Pt adatoms is similar to that of graphite surface while the Rh adatoms create states similar to that of the graphite defects. Entrapment dominates the Pt adatoms while polarization dominates the Rh adatoms while the adatoms bonds become shorter and stronger than those in the bulk. Table 1 also shows the effective CN, bond length and bond energy of the Pt and Rh adatoms in comparison with bulk values [28].

This finding clarifies unambiguously why the undercoordinated Pt and Rh adatoms serve differently as efficient catalysts. If there is additional occupied state (unoccupied) at the top of the valence band of a specimen, it will be easy to lose (gain) electrons and serve as a donor (acceptor) in catalytic reaction. Therefore, the Pt is an acceptor-like because of the entrapment while the Rh a donor-like because of the polarization. From this perspective, graphite surface and defect shall perform differently for potential catalysts.

Using the ZPS we can identify why the interface alloys of AgPd and CuPd function differently as good catalysts. For example, CuPd is active in CO and alkene oxidization and becomes a fancy catalyst in NO reduction [29]; AgPd alloy is more suitable for hydrogen reaction and permeation [30,31]. Khanuja et al. [32] conducted UPS and XPS measurements on AgPd and CuPd thin films as Cu(2 nm) and Ag(2 nm) thin films were deposited onto Pd(10 nm) substrate before and after annealing for alloy formation.

The ZPS in Fig. 2 shows that interface alloying cause entrapment of the CuPd and polarization of AgPd, which coined with the ZPS of the Pt and the Rh adatoms, respectively. The valence bands of the alloys show the same trend of entrapment and polarization consistently. Table 2 summarizes information derived from the ZPS regarding interface induced energy shift, $\Delta E_\nu(I) - \Delta E_\nu(B)$, potential well depth, $\gamma = [\Delta E_\nu(I)\ \Delta E_\nu(B)]/\Delta E_\nu(B)$. $\gamma > 1$, entrapment becomes dominance, otherwise, polarization dominance.

We present a powerful, yet simple ZPS method that has enabled purification of the coordination-resolved, local, and quantitative information of electronic binding energy associated ill-coordinated atoms. Outcome clarifies unambiguously the catalytic nature of Pt and Rh adatoms and the AgPd and CuPd alloys, which is beyond any other available approaches.

**Table 2**
Alloying induced energy shift $\Delta E_\nu(I) - \Delta E_\nu(B)$, potential well depth $\gamma$, and the interface energy shift $\Delta E_\nu(I)$ with respect to the specific energy level of an isolated atom.

| Alloy | $E$-levels | $\Delta E_\nu(B)$ | $E_\nu(0)$ | $\Delta E_\nu(I) - \Delta E_\nu(B)$ | $\gamma$ | $\Delta E_\nu(I)$ |
|---|---|---|---|---|---|---|
| Cu–Pd | Cu $2p_{3/2}$ | 1.70 | 931.00 | 1.62 | 1.9529 | 3.32 |
| | Pd $3d_{5/2}$ | 3.98 | 330.34 | 1.57 | 1.3945 | 5.55 |
| Ag–Pd | | | | −1.22 | 0.6935 | 2.76 |
| | Ag $3d_{5/2}$ | 4.63 | 333.02 | −1.18 | 0.7451 | 3.45 |

## Funding

Financial support from NSF (nos. 11172254, 11242005) China is gratefully acknowledged.

## References

[1] Jehng JM, Chen CM. Amination of polyethylene glycol to polyetheramine over the supported nickel catalysts. Catal Lett 2001;77(1–3):147–54.
[2] Lee CL, Huang YC, Kuo LC. High catalytic potential of Ag/Pd nanoparticles from self-regulated reduction method on electroless Ni deposition. Electrochem Commun 2006;8(6):1021–6.
[3] Xu Y, He KT, Schmucker SW, Guo Z, Koepke JC, Wood JD, et al. Inducing electronic changes in graphene through silicon (100) substrate modification. Nano Lett 2011;11(7):2735–42.
[4] He KT, Koepke JC, Barraza-Lopez S, Lyding JW. Separation-dependent electronic transparency of monolayer graphene membranes on III–V semiconductor substrates. Nano Lett 2010;10(9):3446–52.
[5] Sun CQ. Oxidation electronics: bond–band–barrier correlation and its applications. Prog Mater Sci 2003;48(6):521–685.
[6] Fister TT, Fong DD, Eastman JA, Iddir H, Zapol P, Fuoss PH, et al. Total-reflection inelastic X-ray scattering from a 10-nm thick $La_{0.6}Sr_{0.4}CoO_3$ thin film. Phys Rev Lett 2011;106(3):037401.
[7] Speranza G, Minati L. The surface and bulk core line's in crystalline and disordered polycrystalline graphite. Surf Sci 2006;600(19):4438–44.
[8] Yang DQ, Sacher E. Carbon 1s X-ray photoemission line shape analysis of highly oriented pyrolytic graphite: the influence of structural damage on peak asymmetry. Langmuir 2006;22(3):860–2.
[9] Aruna I, Mehta BR, Malhotra LK, Shivaprasad SM. Size dependence of core and valence binding energies in Pd nanoparticles: interplay of quantum confinement and coordination reduction. J Appl Phys 2008;104(6):064308.
[10] Sun CQ. Atomic scale purification of electron spectroscopic information (USA patent: publication: Dec, 22 2011: WO 2011/159252); 2011 [USA].
[11] Balasubramanian T, Andersen JN, Wallden L. Surface-bulk core-level splitting in graphite. Phys Rev B 2001;64:205420.
[12] Sun CQ, Bai HL, Li S, Tay BK, Jiang EY. Size-effect on the electronic structure and the thermal stability of a gold nanosolid. Acta Mater 2004;52(2):501–5.
[13] Sun CQ. Dominance of broken bonds and nonbonding electrons at the nanoscale. Nanoscale 2010;2(10):1930–61.
[14] Omar MA. Elementary solid state physics: principles and applications. New York: Addison-Wesley; 1993.
[15] Sun CQ, Sun Y, Nie YG, Wang Y, Pan JS, Ouyang G, et al. Coordination-resolved c-c bond length and the C 1s binding energy of carbon allotropes and the effective atomic coordination of the few-layer graphene. J Chem Phys C 2009;113(37):16464–7.
[16] Sun CQ, Fu SY, Nie YG. Dominance of broken bonds and unpaired nonbonding pi-electrons in the band gap expansion and edge states generation in graphene nanoribbons. J Chem Phys C 2008;112(48):18927–34.
[17] Sun CQ, Bai HL, Tay BK, Li S, Jiang EY. Dimension, strength, and chemical and thermal stability of a single c-c bond in carbon nanotubes. J Phys Chem B 2003;107:7544–6.
[18] Falvo MR, Clary GJ, Taylor RM, Chi V, Brooks FP, Washburn S, et al. Bending and buckling of carbon nanotubes under large strain. Nature 1997;389:582–4.
[19] Wong EW, Sheehan PE, Lieber CM. Nanobeam mechanics: elasticity, strength, and toughness of nanorods and nanotubes. Science 1997;277(5334):1971–5.
[20] An B, Fukuyama S, Yokogawa K, Yoshimura M. Surface superstructure of carbon nanotubes on highly oriented pyrolytic graphite annealed at elevated temperatures. Jpn J Appl Phys 1998;37(Part 1, No. 6B):3809–11.
[21] Ki-jeong K, Hangil L, Jae-Hyun C, Young-Sang Y, Junghun C, Hankoo L, et al. Scanning photoemission microscopy of graphene sheets on $SiO_2$. Adv Mater 2008;20(19):3589–91.
[22] Qin W, Wang Y, Huang YL, Zhou ZF, Yang C, Sun CQ. Bond order resolved 3d(5/2) and valence band chemical shifts of Ag surfaces and nanoclusters. J Phys Chem A 2012;116(30):7892–7.
[23] Zhang X, Nie YG, Zheng WT, Kuo JL, Sun CQ. Discriminative generation and hydrogen modulation of the Dirac-Fermi polarons at graphene edges and atomic vacancies. Carbon 2011;49(11):3615–21.

Please cite this article in press as: Nie Y, et al., Catalytic nature of under- and hetero-coordinated atoms resolved using zone-selective photoelectron spectroscopy (ZPS), Vacuum (2013), http://dx.doi.org/10.1016/j.vacuum.2013.07.025

[24] Sun CQ, Wang Y, Nie YG, Mehta BR, Khanuja M, Shivaprasad SM, et al. Interface charge polarization and quantum trapping in AgPd and CuPd bimetallic alloy catalysts. Phys Chem Chem Phys 2010;12:3131–5.
[25] Ugeda MM, Brihuega I, Guinea F, Gómez-Rodríguez JM. Missing atom as a source of carbon magnetism. Phys Rev Lett 2010;104:096804.
[26] Baraldi A, Bianchettin L, Vesselli E, de Gironcoli S, Lizzit S, Petaccia L, et al. Highly under-coordinated atoms at Rh surfaces: interplay of strain and coordination effects on core level shift. N J Phys 2007;9(143):12.
[27] Bianchettin L, Baraldi A, de Gironcoli S, Vesselli E, Lizzit S, Petaccia L, et al. Core level shifts of undercoordinated Pt atoms. J Chem Phys 2008;128(11):114706.
[28] Kittel C. Intrduction to Solid State Physics. 8 ed. New York: John Willey & Sons, Inc; 2005.
[29] Reilly JP, Barnes CJ, Price NJ, Bennett RA, Poulston S, Stone P, et al. The growth mechanism, thermal stability, and reactivity of palladium mono- and multilayers on Cu(110). J Phys Chem B 1999;103(31):6521–32.
[30] Amandusson H, Ekedahl LG, Dannetun H. Hydrogen permeation through surface modified Pd and PdAg membranes. J Membr Sci 2001;193(1):35–47.
[31] Efremenko I, Matatov-Meytal U, Sheintuch M. Hydrodenitrification with PdCu catalysts: catalyst optimization by experimental and quantum chemical approaches. Isr J Chem 2006;46(1):1–15.
[32] Khanuja M, Mehta BR, Shivaprasad SM. Geometric and electronic changes during interface alloy formation in Cu/Pd bimetal layers. Thin Solid Films 2008;516:5435–9.

Please cite this article in press as: Nie Y, et al., Catalytic nature of under- and hetero-coordinated atoms resolved using zone-selective photoelectron spectroscopy (ZPS), Vacuum (2013), http://dx.doi.org/10.1016/j.vacuum.2013.07.025